



High angular momentum hot differentially rotating equilibrium star evolutions in conformally flat spacetime

Patrick Chi-Kit Cheong ^{1,2,*} Nishad Muhammed ³ Pavan Chawhan ³ Matthew D. Duez ³
Francois Foucart ¹ Lawrence E. Kidder ⁴ Harald P. Pfeiffer ⁵ and Mark A. Scheel ⁶

¹*Department of Physics & Astronomy, University of New Hampshire, 9 Library Way, Durham NH 03824, USA*

²*Department of Physics, University of California, Berkeley, Berkeley, CA 94720, USA*

³*Department of Physics & Astronomy, Washington State University, Pullman, Washington 99164, USA*

⁴*Cornell Center for Astrophysics and Planetary Science, Cornell University, Ithaca, New York 14853, USA*

⁵*Max Planck Institute for Gravitational Physics (Albert Einstein Institute), Am Mühlenberg 1, D-14476 Potsdam, Germany*

⁶*Theoretical Astrophysics, Walter Burke Institute for Theoretical Physics, California Institute of Technology, Pasadena, California 91125, USA*

(Dated: July 24, 2024)

The conformal flatness approximation to the Einstein equations has been successfully used in many astrophysical applications such as initial data constructions and dynamical simulations. Although it has been shown that full general relativistic strongly differentially rotating equilibrium models deviate by at most a few percent from their conformally flat counterparts, whether those conformally flat solutions remain stable has not been fully addressed. To further understand the limitations of the conformal flatness approximation, in this work, we construct spatially-conformally-flat hot hypermassive neutron stars with post-merger-like rotation laws, and perform conformally flat evolutions and analysis over dynamical timescales. We find that enforcing conformally-flat spacetime could change the equilibrium of quasi-toroidal models with high angular momentum for $J \gtrsim 9 GM_{\odot}^2/c$ compared to fully general relativistic cases. In contrast, all the quasi-spherical models considered in this work remain stable even with high angular momentum $J = 9 GM_{\odot}^2/c$. Our investigation suggests that the quasi-spherical models are suitable initial data for long-lived hypermassive neutron star modeling in conformally flat spacetime.

I. INTRODUCTION

The detection of a binary neutron star merger on 17 August 2017 has laid a milestone in multi-messenger astronomy. This event was observed by the coincident detections of gravitational waves GW170817 [1], the short gamma-ray burst GRB170817A [2], and in other spectral bands [3]. Even though this groundbreaking multimessenger detection has confirmed our basic understanding of neutron star mergers [4, 5], details of the post-merger evolution are poorly understood. A hypermassive neutron star, which is expected to be hot and supported by strong differential rotation, is one of the possible outcomes of binary neutron star merger. Studying hypermassive neutron star helps us to further understand the nature of the central engine of the relativistic jets [2, 6] and kilonova transients [7–10].

Detailed investigations of the post-merger phase over dynamical and secular timescales are extremely challenging yet significant. Not only does one need to solve Einstein field equations and general-relativistic magneto-hydrodynamics self-consistently [5], neutrino microphysics is also required [11]. Moreover, to better understand the post-merger observational signatures, seconds-long simulations are required. Hence, any simplification of the simulations is highly desirable.

The spatially conformally flat spacetime approximation [12–14] has shown to be useful for modeling neutron

star mergers. Binary neutron star merger simulations based on the conformally flat approximation have been successfully carried out (e.g. [15–20], see also the applications in the context of core-collapse supernovae [21–23] and isolated neutron stars [24–34]). In addition, it has been shown in fully general relativistic simulations that long-lived neutron star merger remnants are qualitatively axisymmetric, and the corresponding spacetime is nearly conformally flat [35, 36]. Mapping such post-merger profiles by assuming conformally flat conditions onto other evolution codes that impose different symmetries or with different input physics has been done recently [35, 36]. Specifically, the multigrid based conformally-flat spacetime solver of Gmunu [37, 38] has been demonstrated to be very effective for the studies of long-lived post-merger neutron star merger remnants over secular timescales [36].

Understanding the limitation of the conformally flat spacetime approximation in the context of hypermassive neutron stars is critical. Despite the success in neutron star modeling (e.g. [15–20]), the conformally flat condition is ultimately an approximation. This approximation is no longer valid in the case of a Kerr black hole [39, 40], and it may also fail with systems that have extreme rotation or high angular momentum. Studies have shown that the local and integrated quantities are at most a few percent difference between fully general relativistic and conformally flat differentially rotating equilibrium models [41–44]. However, whether the full and conformally flat solutions share the same properties of dynamical and secular stabilities is not clearly addressed. Re-

* patrick.cheong@berkeley.edu; N3AS Postdoctoral fellow

cently, the conformally flat approximated dynamical evolutions of quasi-toroidal models with the J -constant rotation law [45] with polytropic equation of state has been carried out [46]. Nevertheless, the rotation law considered in [46] is very different from that of post-merger remnants. It is still unclear whether post-merger like hypermassive neutron stars can be accurately modelled under the conformal flatness approximation.

In this work, we investigate the limitations of the conformally-flat approximation in high angular momentum post-merger-like hypermassive neutron star modeling. In particular, we construct spatially-conformally-flat post-merger-like hot hypermassive neutron stars, and perform evolutions and analysis over dynamical timescales. We find that the stellar profiles of conformally-flat quasi-toroidal models with high angular momentum for $J \gtrsim 9 GM_{\odot}^2/c$ can be distorted noticeably over dynamical timescales even in fully general relativistic evolutions. However, the fully general relativistic variant of such stars remain stable in fully general relativistic evolutions within the time we simulated. This implies that conformally-flat approximation either makes such high angular momentum star not an equilibrium or makes it an unstable equilibrium. On the other hand, all the quasi-spherical models considered in this work remain stable even with high angular momentum $J = 9 GM_{\odot}^2/c$. Our study suggests that the quasi-spherical models are better choice to be used as hypermassive neutron star modeling because of their rotation properties and stabilities.

The paper is organised as follows. In section II we outline the methods we used in this work. The results are presented in section III. This paper ends with a discussion in section IV. Unless explicitly stated, we use the units in which the speed of light c , gravitational constant G , solar mass M_{\odot} are all equal to one ($c = G = M_{\odot} = 1$).

II. METHODS

A. Initial conditions

Conformally flat, axisymmetric, differentially rotating hot neutron stars in quasi-equilibrium are constructed using the `RotNS` code [47], and serve as our initial data. `RotNS` [47] was used to construct equilibrium sequences of rotating polytropes in general relativity. The code has been recently updated to support tabulated equations of state and the 4-parameter rotation law of Uryū *et al.* [48]. For the implementation details, we refer readers to [49]. Below, we will only highlight the key setup of the initial data construction.

Although `RotNS` [47] is a fully general relativistic code, the spatially-conformally-flat conditions can easily be enforced by imposing an additional condition of the metric potentials, as shown in [41–44]. Here we adopt the same modification in `RotNS` to construct conformally flat initial data. Unless explicitly stated, all the initial data are

constructed in conformally-flat spacetime.

To construct merger-like hypermassive neutron star profiles, we adopt the 4-parameter rotation law of Uryū *et al.* [48]. In particular, we implement the following rotation law,

$$\Omega(j; \Omega_c) = \Omega_c \frac{1 + [j / (B^2 \Omega_c)]^p}{1 + [j / (A^2 \Omega_c)]^{q+p}}, \quad (1)$$

where j is the specific angular momentum, Ω_c is the central angular velocity of the star, while A , B , q , and p are parameters. In this work, we choose $p = 1$ and $q = 3$. Note that this rotation profile is non-monotonic, with the maximum angular velocity Ω_{\max} between the centre and surface. The characteristic of the models can be controlled by specifying parameters A and B . Alternatively, parameters A and B can be obtained by fixing angular velocity ratios Ω_{\max}/Ω_c and $\Omega_{\text{eq}}/\Omega_c$ [43, 44, 48], where Ω_{eq} is the equatorial angular velocity of the star. Different choices of the angular velocity ratios can result in either quasi-toroidal or quasi-spherical models.

In this work, we consider two sets of the ratios $\{\Omega_{\max}/\Omega_c, \Omega_{\text{eq}}/\Omega_c\}$, namely: (i) $\{2, 0.5\}$ which results in quasi-toroidal models, and (ii) $\{1.6, 1\}$ which results in quasi-spherical models (see figure 1 for examples of the rest mass density profiles of both types of stars). They can be classified as type C and type A solutions according to [50]. Note that the latter set of the ratios are chosen to match the results of the numerical relativity simulations of binary neutron star mergers (e.g. [51, 52], see [43, 44]). Therefore, the quasi-spherical type models are by construction more “post-merger-like” compared to quasi-toroidal models.

All the equilibrium models in this work are constructed with equation of state DD2 [53] with a constant entropy per baryon $s = 1 k_B/\text{baryon}$ and in neutrinoless β -equilibrium. The temperature is roughly 30 MeV at the centre of the star. Note that, such choice of entropy profile and the resulting temperature profile does not match the numerical relativity simulations, where the temperature at the centre is expected to be lower than the surface. Nevertheless, we consider only the constant entropy profile for simplicity. The investigations of different choice of entropy profiles will be left as future work. The resolution of the compacted radius and angular grid (see their definitions in [47]) in `RotNS` is 600×600 .

B. Simulation setup

We employ the general relativistic magnetohydrodynamics code `Gmumu` [37, 38, 54–56] to evolve the neutron star models in dynamical conformally-flat spacetime. All the simulations here are axisymmetric (i.e. 2-dimensional) in cylindrical coordinates (R, z) , where the computational domain covers $0 \leq R \leq 120$ and $0 \leq z \leq 120$, with the resolution $n_R \times n_z = 128 \times 128$ and allowing 6 AMR levels. The finest grid size at the centre

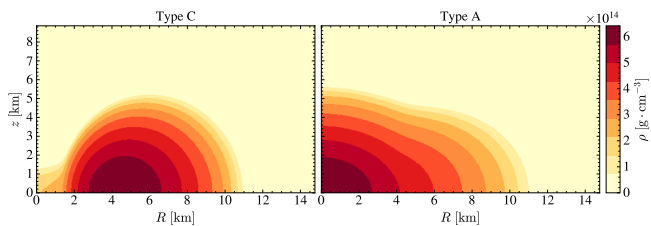


FIG. 1. Two-dimensional rest mass density profiles ρ in the units of $[\text{g} \cdot \text{cm}^{-3}]$ of the rotating neutron star models. *Left panel:* Quasi-toroidal (type C) model with $\{\Omega_{\text{max}}/\Omega_c = 2, \Omega_{\text{eq}}/\Omega_c = 0.5\}$. This star has the angular momentum $J = 11 GM_{\odot}^2/c$ with the maximum energy density $\epsilon_{\text{max}} = 7.073 \times 10^{14} \text{ g} \cdot \text{cm}^{-3}$. *Right panel:* Quasi-spherical (type A) model with $\{\Omega_{\text{max}}/\Omega_c = 1.6, \Omega_{\text{eq}}/\Omega_c = 1\}$. This star has the angular momentum $J = 9 GM_{\odot}^2/c$ with the maximum energy density $\epsilon_{\text{max}} = 9.411 \times 10^{14} \text{ g} \cdot \text{cm}^{-3}$.

of the star is $\Delta R = \Delta z \approx 43.27 \text{ m}$. The refinement is fixed after the initialisation since we do not expect the stars expand significantly.

Our simulations adopt Harten, Lax and van Leer (HLL) approximated Riemann solver [57], 3rd-order reconstruction method PPM [58] and 3rd-order accurate SSPRK3 time integrator [59]. Finite temperature equation of state DD2 [53] is used for the evolutions. Although neutrinos are not included, the electron fraction Y_e is evolved in these simulations.

The rest-mass density of the atmosphere ρ_{atmo} is set to be $10^{-10} \rho_{\text{max}}(t=0)$. For anywhere that the matter has rest-mass density lower than ρ_{atmo} , we reset the rest-mass density of those regions to be $0.2\rho_{\text{atmo}}$, and zero the velocities (i.e. $v^i = 0$). As a result, the angular velocity $\Omega \equiv \alpha v^\phi - \beta^\phi$ has a sudden drop at the neutron star surface at $t = 0$ (see e.g. figure 3). These areas will be filled with low density gas that rotates with similar angular velocity as soon as the simulation started, and do not affect the dynamics of the neutron star because of the ultra-low rest-mass density.

To initialise the simulations, we map the conservative variables of the stars into **Gmunu**, and solve the metric again with the multigrid metric solver [37, 38]. This approach can also be applied on fully general relativistic profiles, which was used in [35, 36].

III. RESULTS

A. Sequences of equilibrium models

Figure 2 shows the gravitational mass M_{grav} versus maximum energy density ϵ_{max} of constant angular momentum sequences constructed in this work. Note again that the spatial conformally flat condition is enforced in all the sequences reported here. Circles and diamonds mark the dynamically evolved models without introducing perturbations. The diamonds refer to the models

presented in detail in figure 3, 4 and 7. None of the simulations presented here collapse as black holes. However, we note that these non-collapsing models are not necessarily stable, see further discussions in section III B and III C below.

The left panel of figure 2 shows quasi-toroidal (type C) models with $\{\Omega_{\text{max}}/\Omega_c = 2, \Omega_{\text{eq}}/\Omega_c = 0.5\}$, where the angular momentum J ranges from 3 to $11 GM_{\odot}^2/c$. The J -constant turning points are observed in all the quasi-toroidal sequences, which are marked with black crosses in the plot. According to the turning point criterion [45], the J -constant turning points mark the onset of instability. However, this is not an exact threshold to collapse. The situation becomes more complicated for differentially rotating cases. The stability and maximum mass of differentially rotating stars with J -constant rotation law [45] has been studied [46, 60, 61]. More recently, Muhammed *et al.* [49] shows that the turning point criterion seems to also hold in the cases of Uryū *et al.* [48] rotation law. In this work, we only dynamically evolve the models that have smaller maximum energy density ϵ_{max} than the J -constant turning points.

The right panel of figure 2 on the other hand shows the quasi-spherical (type A) model with $\{\Omega_{\text{max}}/\Omega_c = 1.6, \Omega_{\text{eq}}/\Omega_c = 1\}$, where the angular momentum J ranges from 3 to $9 GM_{\odot}^2/c$. Unlike the quasi-toroidal cases, we do not observe J -constant turning points in these sequences. As the maximum energy density ϵ_{max} goes beyond the plotted values, the **RotNS** code fails to converge. This behaviour agrees with the discussion in the section 3.2 in [44]. The origin of this issue is still unknown, which is beyond the scope of this work and will be investigated in a future study.

B. Evolutions of quasi-toroidal profiles

In this subsection, we present some evolutions of the quasi-toroidal (type C) models with different angular momentum J and maximum energy density ϵ_{max} . All the models considered here have lower maximum energy density ϵ_{max} than the J -constant turning points. We do not introduce any perturbations into the evolutions. Since all the low angular momentum cases are found to be stable and trivial, in this section we discuss only the high angular momentum cases (i.e. $J \geq 9$).

Figure 3 compares the dynamical evolutions of the quasi-toroidal (type C) models with angular momentum $J = 9$ with different maximum energy densities ϵ_{max} . In all cases, the maximum rest mass densities ρ_{max} oscillate, and gradually relax to a slightly lower value. For the high maximum energy density $\epsilon_{\text{max}} = 1.0245 \times 10^{15} \text{ g} \cdot \text{cm}^{-3}$ case, the final central rest mass density $\rho_c(t = 20 \text{ ms})$ is about 18% smaller than the initial value, which is not ignorable and indicates that the star migrates into another configuration. The rest mass density ρ and the angular velocity Ω along R -axis (i.e. $z = 0$) at the end of the simulation ($t = 20 \text{ ms}$) are significantly distorted except

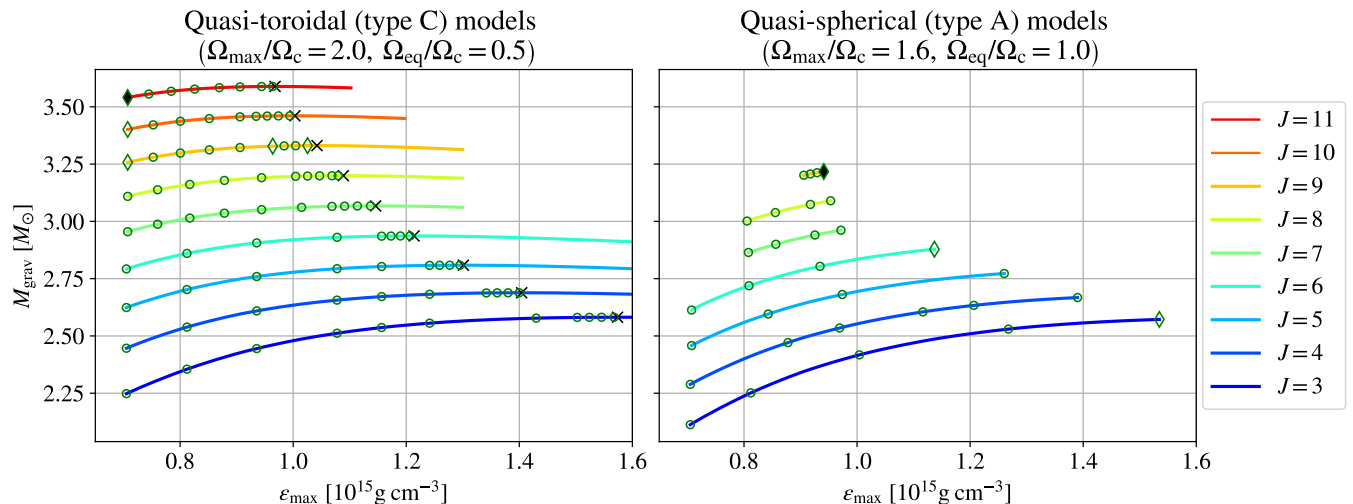


FIG. 2. Gravitational mass M_{grav} versus maximum energy density ϵ_{max} for various constant angular momentum sequences. Circles and diamonds mark the dynamically evolved models without introducing perturbations. The diamonds refer to the models presented in detail in figure 3, 4 and 7. The black diamonds are the two cases presented in figure 1. None of the simulations presented here collapse as black holes. *Left panel:* Quasi-toroidal (type C) model with $\{\Omega_{\text{max}}/\Omega_c = 2.0, \Omega_{\text{eq}}/\Omega_c = 0.5\}$. The angular momentum J ranges from 3 to 11 GM_{\odot}^2/c . The J -constant turning points are marked with black crosses. We find that models with high angular momentum (i.e. $J \gtrsim 9$) fail to preserve their stellar profiles, see figure 3 and 4 and the discussions in section III B. *Right panel:* Quasi-spherical (type A) model with $\{\Omega_{\text{max}}/\Omega_c = 1.6, \Omega_{\text{eq}}/\Omega_c = 1.0\}$. The angular momentum J ranges from 3 to 9 GM_{\odot}^2/c . In this type of the models, we do not observe J -constant turning points. The RotNS code fails to converge when the maximum energy density goes beyond the plotted values, which agrees with [44]. All the dynamically evolved models remain stable up to 20 ms evolutions.

the low maximum energy density case. The distortions are stronger in the higher maximum energy density ϵ_{max} cases. Although none of these neutron stars collapse to black holes, the medium and high energy density cases were not stable against the evolution up to 20 ms.

Figure 4 compares the dynamical evolutions of also the quasi-toroidal models with maximum energy density $\epsilon_{\text{max}} = 7.073 \times 10^{14} \text{ g} \cdot \text{cm}^{-3}$ with high angular momentum $J \geq 9$. The evolutions of the rest mass densities behave similarly, i.e. they oscillate, and gradually relax to a lower value. The higher the angular momentum J is, the stronger the distortion of the rest mass density ρ and the angular velocity Ω profiles. Although the maximum energy density of all the models considered here are noticeably lower than the J -constant turning points, we found that the angular velocity profiles $\Omega(R, z)$ are not preserved in some high angular momentum cases. For instance, in the highest angular momentum $J = 11$ case, the central rest mass density ρ_c decrease significantly by about 20% compared to the initial value. Also, the angular velocity profile $\Omega(R, z = 0)$ changes significantly at the centre of the stars, the rotation law of Uryū *et al.* [48] is violated. Both the central and maximum angular velocities oscillate quasi-periodically with large amplitudes, the angular velocities can sometime be a few times higher than the initial values during the evolutions. Note again that all the models presented in this plot are the least massive models at a given angular momentum (i.e. far from the J -turning points), such strong oscillations and

deformations of the stars are unexpected.

1. Comparison to fully general relativistic cases

To better understand the origin of the non-stable behaviour, we further compare different combinations of conformally-flat and fully general relativistic initial profiles and evolutions of selected quasi-toroidal (type C) models. In this section, we focus on the quasi-toroidal (type C) model with maximum energy density $\epsilon_{\text{max}} = 7.073 \times 10^{14} \text{ g} \cdot \text{cm}^{-3}$ with angular momentum $J = 11$. The Spectral Einstein Code (SpEC) [62] is used for the fully general relativistic evolutions. The details of the numerical setup in SpEC can be found at [49, 63].

In this subsection, we consider four cases, namely, (i) conformally-flat initial data with conformally-flat evolution; (ii) general relativistic initial data with conformally-flat evolution; (iii) conformally-flat initial data with fully general relativistic evolution; and (iv) general relativistic initial data with fully general relativistic evolution. One may argue that it is not necessary to consider case (ii) since it is more-or-less similar to case (i). After all, non-spherically symmetric full general relativistic initial data is in general not conformally flat, there is no self-consistent way to map such initial data into a conformally-flat evolution code. To evolve such star, we solve the conformally-flat metric equations with the conserved variables of the fully general relativistic star,

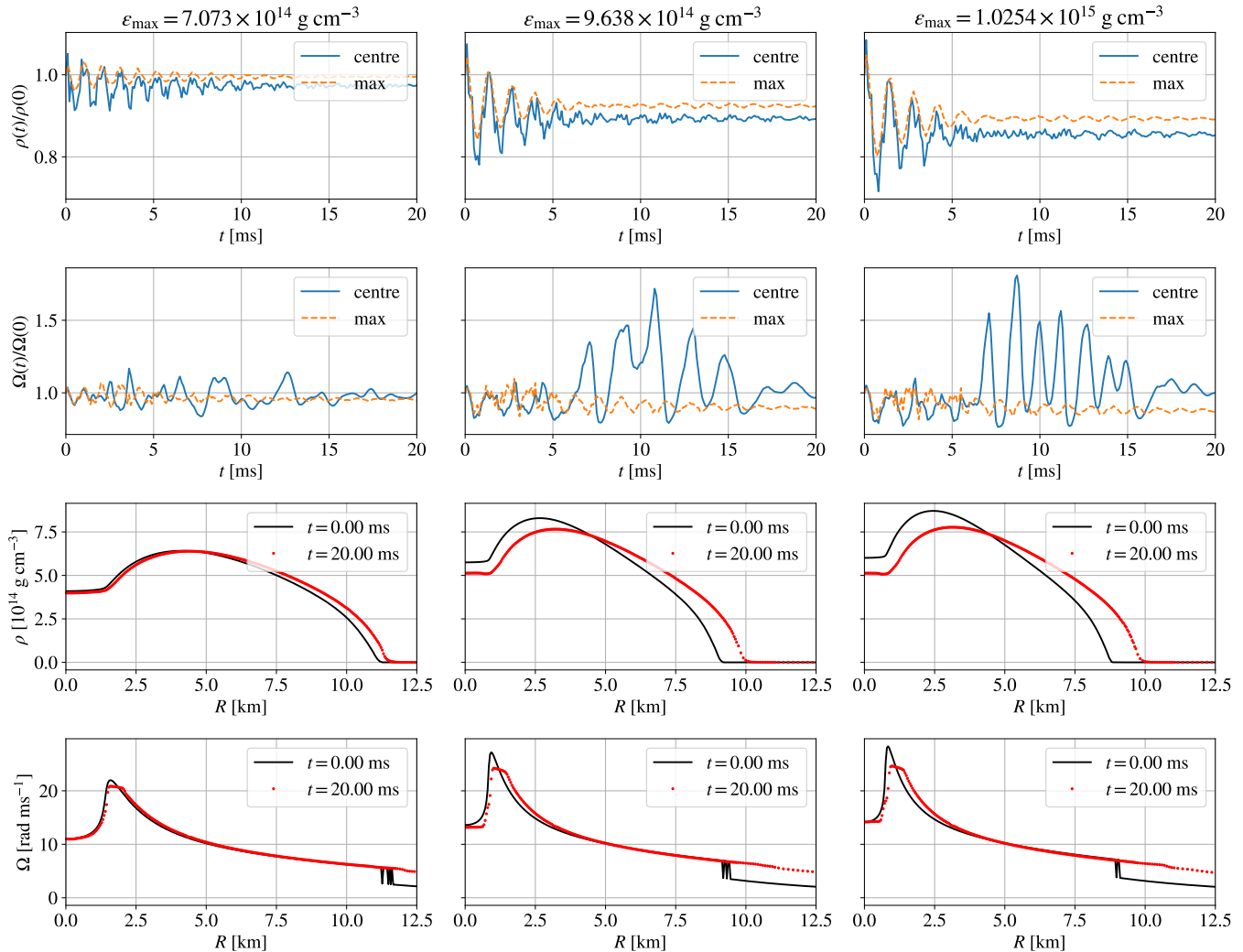
Quasi-toroidal (type C) $J=9$ models ($\Omega_{\max}/\Omega_c = 2.0$, $\Omega_{\text{eq}}/\Omega_c = 0.5$)

FIG. 3. Comparison of the dynamical evolutions of the quasi-toroidal (type C) models with angular momentum $J = 9$ with different maximum energy densities ϵ_{\max} . Three cases are shown in this plot, namely, $\epsilon_{\max} = 7.073 \times 10^{14} \text{ g} \cdot \text{cm}^{-3}$ (left column), $\epsilon_{\max} = 9.638 \times 10^{14} \text{ g} \cdot \text{cm}^{-3}$ (middle column), and $\epsilon_{\max} = 1.0254 \times 10^{15} \text{ g} \cdot \text{cm}^{-3}$ (right column), respectively. The first and second rows show the relative variation of the rest mass densities and angular velocities in time (blue solid lines are for central values while the orange dashed lines are for maximum values). In all cases, the rest mass densities oscillate, and gradually settle to a slightly lower value. The central angular velocity Ω_c oscillate strongly at around 10 ms, but relax back to initial values later. For the high maximum energy density ϵ_{\max} case, the final central rest mass density $\rho_c(t = 20 \text{ ms})$ is about 18% smaller than the initial value. The third and fourth rows compare of the initial (black solid lines) and final ($t = 20 \text{ ms}$, red dots) profiles of the rest mass density ρ and the angular velocity Ω along R -axis (i.e. $z = 0$). The higher the maximum energy density ϵ_{\max} is, the lower of the final maximum rest mass density ρ_{\max} , and stronger the distortion of the rest mass density ρ and the angular velocity Ω profiles. Despite the significant distortions of the rest mass density profiles $\rho(R, z = 0)$, the angular velocity profiles $\Omega(R, z = 0)$ in all the cases considered here are qualitatively preserved.

as discussed in section II B. This is effectively enforcing the initial data to be conformally-flat at the beginning. However, this does not guarantee that the profile will still be an equilibrium. In this work, we nevertheless include this case to discuss the validity of mapping a fully general relativistic profile into a conformally-flat evolution code as in [36].

Comparison of the rest mass densities and angular ve-

locities of the same models with or without conformally flat approximation are shown in figure 5 and 6. In particular, figure 5 shows the absolute values of the relative variation of the central and maximum rest mass densities and angular velocities while figure 6 compares the profiles at $t \approx 6 \text{ ms}$. Interestingly, the conformally-flat initial profile is always unstable even with fully general relativistic evolution. The star remains stable only when the pro-

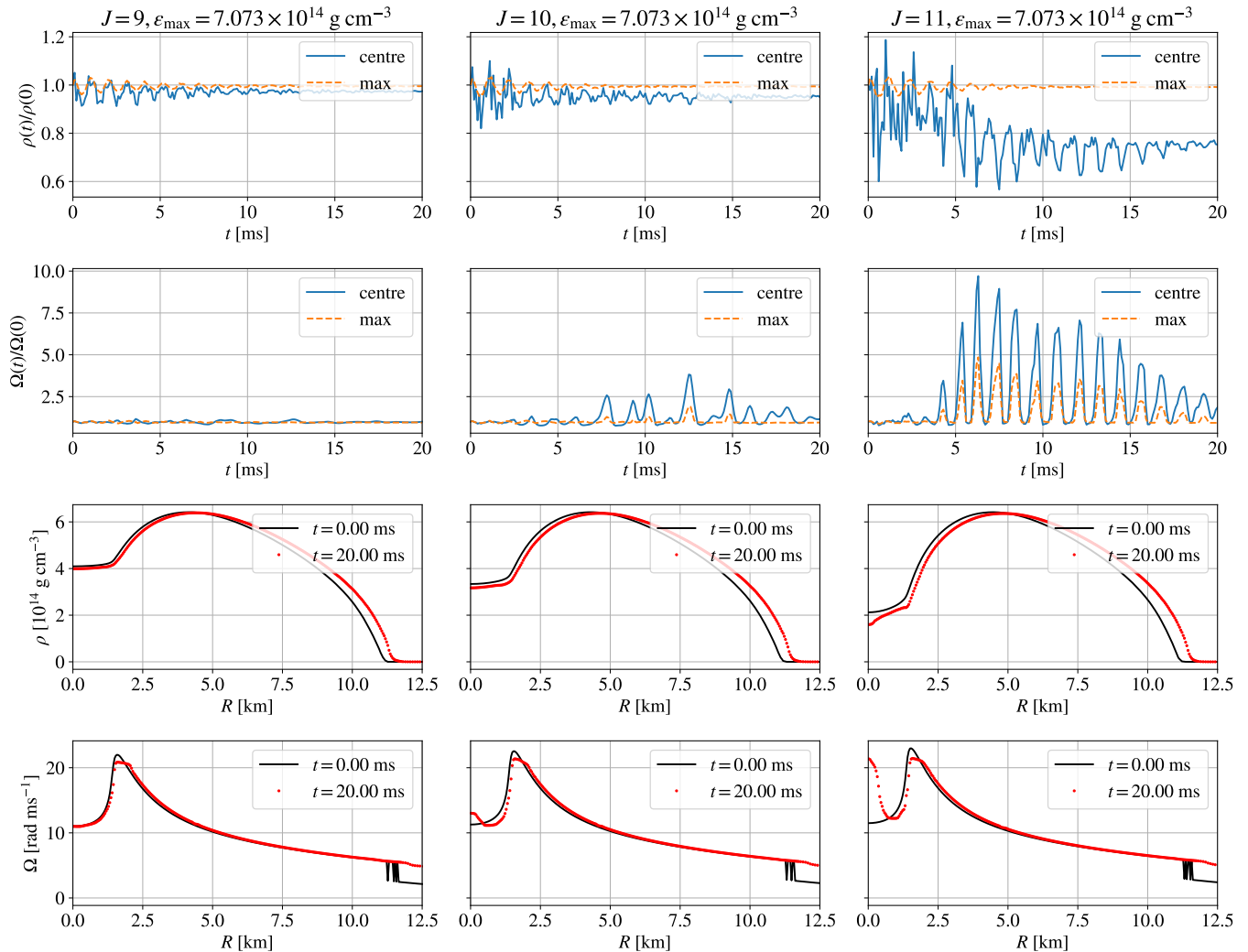
Quasi-toroidal (type C) models ($\Omega_{\max}/\Omega_c = 2.0$, $\Omega_{\text{eq}}/\Omega_c = 0.5$)

FIG. 4. Comparison of the dynamical evolutions of the quasi-toroidal (type C) models with maximum energy density $\epsilon_{\max} = 7.073 \times 10^{14} \text{ g} \cdot \text{cm}^{-3}$ with high angular momentum $J \geq 9$. Three cases are shown in this plot, namely, $J = 9$ (left column), $J = 10$ (middle column), and $J = 11$ (right column), respectively. The first and second rows show the relative variation of the rest mass densities and angular velocities in time (blue solid lines are for central values while the orange dashed lines are for maximum values). The third and fourth rows compare of the initial (black solid lines) and final ($t = 20 \text{ ms}$, red dots) profiles of the rest mass density ρ and the angular velocity Ω along R -axis. The angular velocity profile $\Omega(R, z = 0)$ for $J > 9$ cases change significantly at the centre of the stars, the rotation law of Uryū *et al.* [48] no longer hold. Moreover, in the highest angular momentum $J = 11$ case, although the change of the maximum rest mass density ρ_{\max} is small, the central rest mass density ρ_c decrease by about 20% compare to the initial value. Both the central and maximum angular velocities oscillate quasi-periodically. The amplitudes of the oscillation are very large, the angular velocities can be a few times higher during the evolutions. Note that all the models presented in this plot are the least massive models at a given angular momentum (i.e. far from the J -turning points), such strong oscillations and deformations of the stars are unexpected.

file and evolution are fully general relativistic (case (iv), red lines). This implies that the conformally-flat approximation either makes such high angular momentum star not an equilibrium or makes it an unstable equilibrium.

C. Evolutions of quasi-spherical profiles

In this subsection, we present some evolutions of the quasi-spherical (type A) models with different angular momentum J and maximum energy density ϵ_{\max} . As mentioned, we do not observe any J -constant turning points when we construct the fix angular momentum sequences. Therefore, we simulate models at both ends,

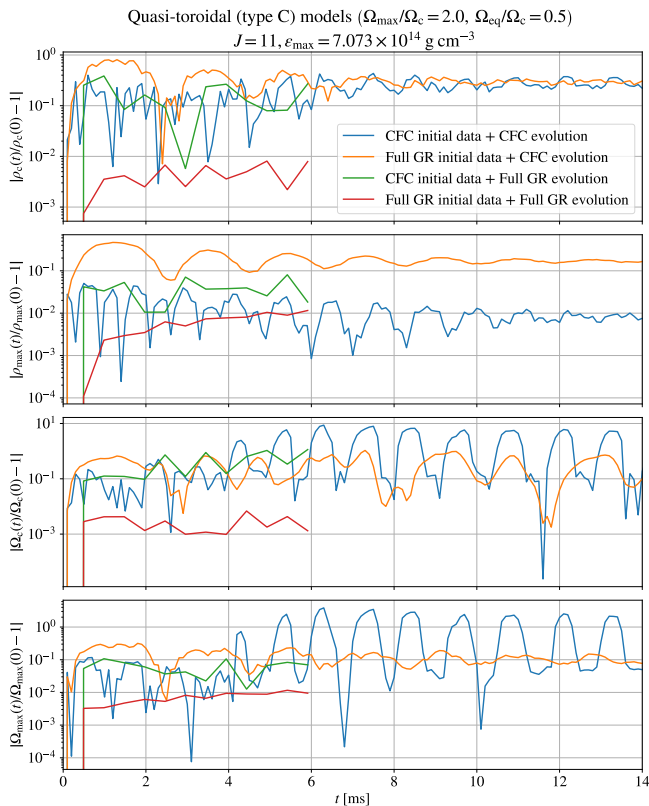


FIG. 5. The relative variation of the central and maximum rest mass densities and angular velocities of the same models with or without conformally flat approximation. The quasi-toroidal (type C) models with maximum energy density $\epsilon_{\max} = 7.073 \times 10^{14} \text{ g} \cdot \text{cm}^{-3}$ with angular momentum $J = 11$ is used in these simulations. All the evolutions have significant deviations except cases where both initial profile and evolution are fully general relativistic (red lines). Although the conformally flat equilibrium solutions have only a few percent deviations from their fully general relativistic counterpart [41–44], the dynamical stabilities of high angular momentum equilibrium models could be changed under conformally flat approximation.

i.e. from low to high maximum energy density ϵ_{\max} .

Figure 7 compares the dynamical evolutions of the quasi-spherical (type A) models with the most massive models at three given angular momentum $J = 3$, $J = 6$ and $J = 9$. Although they are the most extreme type A models we have constructed, all of them are dynamically stable in conformally flat simulations. Indeed, all the simulations we have done (the green circles in the right panel of figure 2) of this type of models remain stable.

IV. DISCUSSION

The goal of this work is to investigate how well the differentially rotating quasi-equilibrium models with high angular momentum remain stable in spatially-conformally-flat simulations. To this end, we have con-

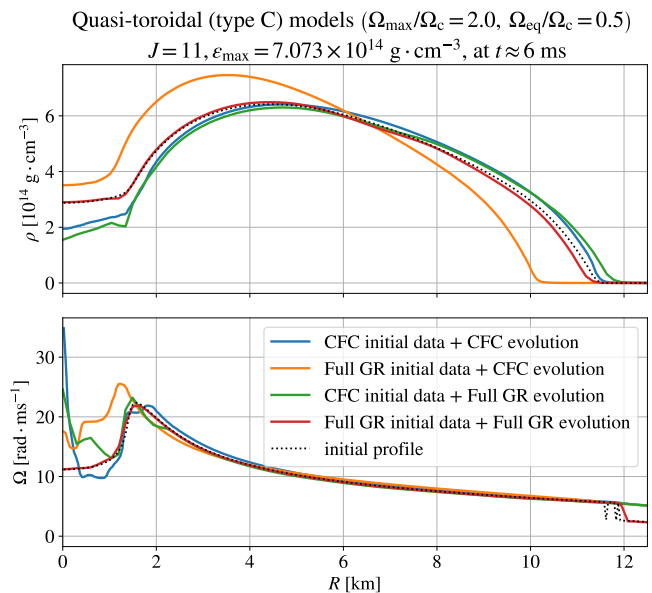


FIG. 6. Comparison of the rest mass density and angular velocity profiles at the beginning ($t = 0$ ms, black dotted lines) and at $t \approx 6$ ms (solid lines) of the same models with or without conformally flat approximation. The quasi-toroidal (type C) models with maximum energy density $\epsilon_{\max} = 7.073 \times 10^{14} \text{ g} \cdot \text{cm}^{-3}$ with angular momentum $J = 11$ is used in these simulations. The profiles are well-preserved only in the case where both initial profile and evolution are fully general relativistic (red lines).

structed both quasi-toroidal and quasi-spherical types of spatially-conformally-flat merger-like hot hypermassive neutron stars. In particular, the “post-merger-like” rotation law of Uryū *et al.* [48] is introduced, and assuming constant entropy per baryon $s = 1 k_B/\text{baryon}$ and in neutrinoless β -equilibrium. We further assess their stability by performing dynamical simulations in conformally flat spacetime using **Gmunu**.

We show that conformally-flat approximation could alter the dynamical stability of the quasi-toroidal models despite only a few percent difference with their fully general-relativistic variation [41–44]. Our simulations show that not all conformally-flat quasi-toroidal models remain dynamically stable even for cases where the maximum energy density ϵ_{\max} is considerably smaller than the J -constant turning points. In high angular momentum (i.e. $J \gtrsim 9$) conformally-flat cases, both the rest mass density and angular velocity can be distorted significantly even with fully general relativistic evolutions. However, this is not the case when both initial profile and evolutions are fully general-relativistic. This implies that conformally-flat approximation either makes such high angular momentum star not an equilibrium or makes it an unstable equilibrium. Mapping these stellar profiles from fully general relativistic simulations to other codes by assuming conformally-flat conditions (e.g. [35, 36]) could result in very different lifetime of the star, and

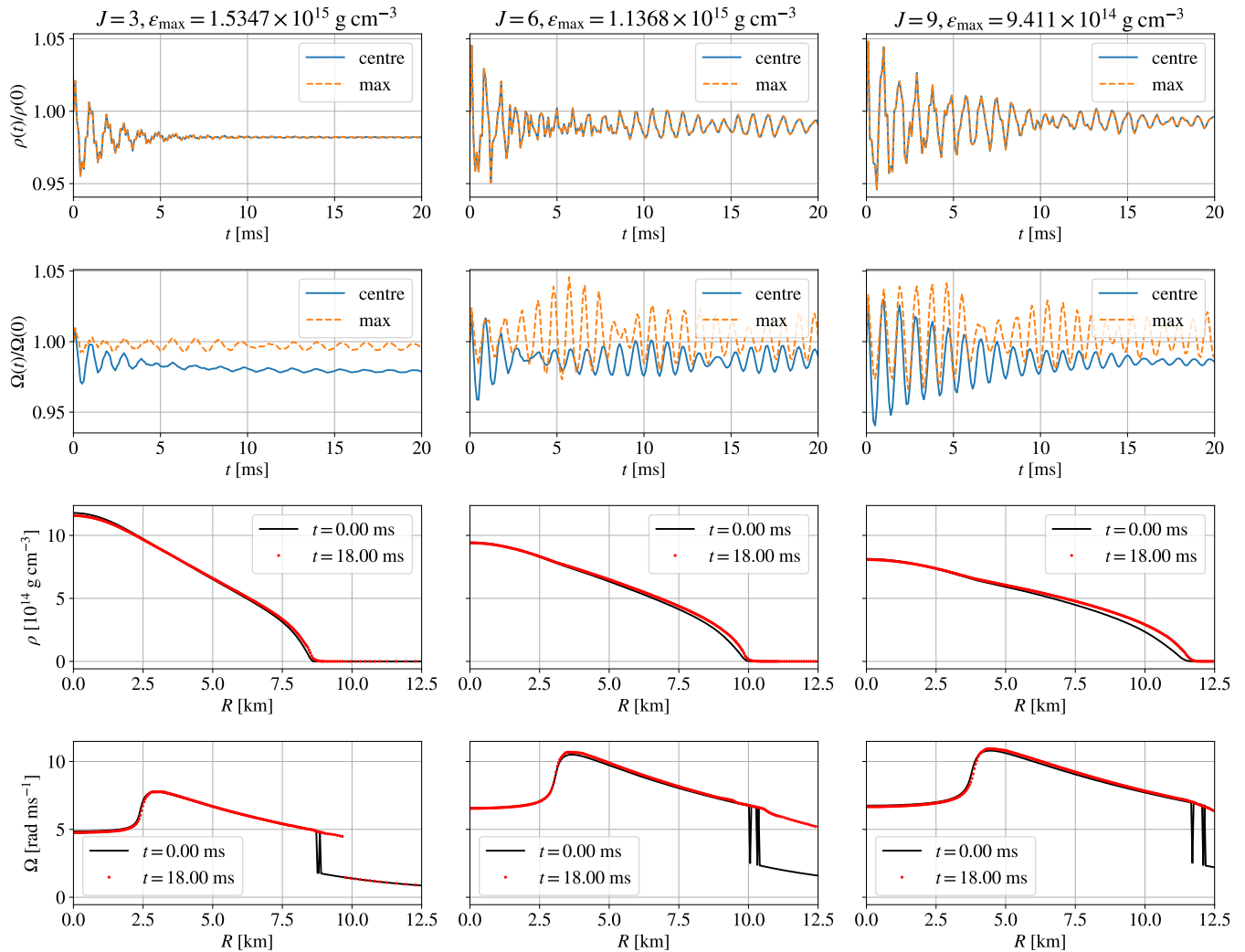
Quasi-spherical (type A) models ($\Omega_{\text{max}}/\Omega_c = 1.6$, $\Omega_{\text{eq}}/\Omega_c = 1.0$)

FIG. 7. Comparison of the dynamical evolutions of the quasi-spherical (type A) models with different maximum energy densities ϵ_{max} and angular momentum J . In this plot, we show the most massive models with three given angular momentum, i.e. $J = 3$ (left column), $J = 6$ (middle column), and $J = 9$ (right column). The first and second rows show the relative variation of the rest mass densities and angular velocities in time (blue solid lines are for central values while the orange dashed lines are for maximum values). The evolutions of the maximum and central rest mass densities ρ are identical in the quasi-spherical models. All the relative variations shown here are within 5%. The third and fourth rows compare of the rest mass density ρ and the angular velocity Ω profiles along R -axis at the beginning ($t = 0$ ms, black solid lines) and a later time $t = 18$ ms (red dots). As shown at the first two rows, the $J = 6$ and $J = 9$ models are not yet relax to stationary states by the end of the simulations ($t = 20$ ms), the oscillation is still noticeable in the scale we are plotting. Such oscillations result in small quasi-periodic distortions of the stellar profiles (e.g. angular velocity Ω). Therefore, instead of plotting the profiles at the end of the simulations, we pick the slightly earlier time (i.e. at $t = 18$ ms) for better visualisations. Unlike the cases in quasi-toroidal (see figure 4 and 3), the profiles are preserved better in this case, and the decrease of the maximum rest mass density ρ is about 2% even for most massive case with the highest angular momentum $J = 9$. These results suggest that these quasi-spherical (type A) models are dynamically stable in conformally flat simulations within 20 ms.

therefore affecting the modeling of the matter outflow. The origin of such behaviour can be better understood by studying its hydrodynamical instability (e.g. [64]), which is left as future work.

On the other hand, unlike the quasi-toroidal models, we show that all the quasi-spherical models considered in

this work remain stable. The quasi-spherical models are not only by construction more post-merger-like compared to the quasi-toroidal models, they are dynamically stable even for the most extreme cases we considered. These properties make them ideal choices for long-lived hyper-massive neutron star modeling. Generating different se-

quences with different parameters (e.g. mass, angular momentum, equation of state) enable us to systemically study how these parameters affect the outcomes of the post-merger. In the future, we will attempt to deliver post-merger modeling with such quasi-spherical models together with magnetic fields and neutrino transport.

ACKNOWLEDGMENTS

P.C.K.C. gratefully acknowledges support from NSF Grant PHY-2020275 (Network for Neutrinos, Nuclear Astrophysics, and Symmetries (N3AS)). F.F. gratefully acknowledge support from the Department of Energy, Office of Science, Office of Nuclear Physics, under contract number DE-AC02-05CH11231 and from the NSF through grant AST-2107932. M.D. gratefully acknowledges support from the NSF through grant PHY-2110287. M.D. and F.F. gratefully acknowledge support from NASA through grant 80NSSC22K0719.

The simulations in this work have been performed on the third UNH supercomputer Marvin, also known as Plasma, which is supported by NSF/MRI program under grant number AGS-1919310. The data of the simulations were post-processed and visualised with yt [65], NumPy [66], pandas [67, 68], SciPy [69] and Matplotlib [70, 71].

Appendix A: Convergence tests

Here we present the convergence tests. The simulations have the same setup as in the paper, except that we introduce initial in-going velocity perturbation. As shown in figure 8. As shown in the plot, the oscillation amplitudes are mostly the same at the very beginning, and gradually decrease as time goes on. At low resolution, the simulations are very diffusive, which relax to the stationary state sooner.

-
- [1] B. P. Abbott, R. Abbott, T. D. Abbott, F. Acernese, K. Ackley, C. Adams, and T. Adams, GW170817: Observation of Gravitational Waves from a Binary Neutron Star Inspiral, *Phys. Rev. Lett.* **119**, 161101 (2017), arXiv:1710.05832 [gr-qc].
 - [2] B. P. Abbott, R. Abbott, T. D. Abbott, F. Acernese, K. Ackley, C. Adams, and T. Adams, Gravitational Waves and Gamma-Rays from a Binary Neutron Star Merger: GW170817 and GRB 170817A, *ApJ* **848**, L13 (2017), arXiv:1710.05834 [astro-ph.HE].
 - [3] B. P. Abbott, R. Abbott, T. D. Abbott, F. Acernese, K. Ackley, C. Adams, and T. Adams, Multi-messenger Observations of a Binary Neutron Star Merger, *ApJ* **848**, L12 (2017), arXiv:1710.05833 [astro-ph.HE].
 - [4] B. D. Metzger, Welcome to the Multi-Messenger Era! Lessons from a Neutron Star Merger and the Landscape Ahead, arXiv e-prints , arXiv:1710.05931 (2017), arXiv:1710.05931 [astro-ph.HE].
 - [5] L. Rezzolla, P. Pizzochero, D. I. Jones, N. Rea, and I. Vidaña, The Physics and Astrophysics of Neutron Stars, *Astrophysics and Space Science Library* **457**, 10.1007/978-3-319-97616-7 (2018).
 - [6] E. Berger, Short-Duration Gamma-Ray Bursts, *ARA&A* **52**, 43 (2014), arXiv:1311.2603 [astro-ph.HE].
 - [7] L.-X. Li and B. Paczyński, Transient Events from Neutron Star Mergers, *ApJ* **507**, L59 (1998), arXiv:astro-ph/9807272 [astro-ph].
 - [8] B. D. Metzger, G. Martínez-Pinedo, S. Darbha, E. Quataert, A. Arcones, D. Kasen, R. Thomas, P. Nugent, I. V. Panov, and N. T. Zinner, Electromagnetic counterparts of compact object mergers powered by the radioactive decay of r-process nuclei, *MNRAS* **406**, 2650 (2010), arXiv:1001.5029 [astro-ph.HE].
 - [9] M. Tanaka, Kilonova/Macronova Emission from Compact Binary Mergers, *Advances in Astronomy* **2016**, 634197 (2016), arXiv:1605.07235 [astro-ph.HE].
 - [10] B. D. Metzger, Kilonovae, *Living Reviews in Relativity* **23**, 1 (2019), arXiv:1910.01617 [astro-ph.HE].
 - [11] F. Foucart, Neutrino transport in general relativistic neutron star merger simulations, *Living Reviews in Computational Astrophysics* **9**, 1 (2023), arXiv:2209.02538 [astro-ph.HE].
 - [12] J. R. Wilson and G. J. Mathews, *Relativistic Numerical Hydrodynamics*, Cambridge Monographs on Mathematical Physics (Cambridge University Press, 2003).
 - [13] J. A. Isenberg, Waveless Approximation Theories of Gravity, *International Journal of Modern Physics D* **17**, 265 (2008), arXiv:gr-qc/0702113 [gr-qc].
 - [14] I. Cordero-Carrión, P. Cerdá-Durán, H. Dimmelmeier, J. L. Jaramillo, J. Novak, and E. Gourgoulhon, Improved constrained scheme for the Einstein equations: An approach to the uniqueness issue, *Phys. Rev. D* **79**, 024017 (2009), arXiv:0809.2325 [gr-qc].
 - [15] R. Oechslin, S. Rosswog, and F.-K. Thielemann, Conformally flat smoothed particle hydrodynamics application to neutron star mergers, *Phys. Rev. D* **65**, 103005 (2002), arXiv:gr-qc/0111005 [gr-qc].
 - [16] A. Bauswein, H. T. Janka, K. Hebeler, and A. Schwenk, Equation-of-state dependence of the gravitational-wave signal from the ring-down phase of neutron-star mergers, *Phys. Rev. D* **86**, 063001 (2012), arXiv:1204.1888 [astro-ph.SR].
 - [17] A. Bauswein, S. Goriely, and H. T. Janka, Systematics of Dynamical Mass Ejection, Nucleosynthesis, and Radioactively Powered Electromagnetic Signals from Neutron-star Mergers, *Astrophys. J.* **773**, 78 (2013), arXiv:1302.6530 [astro-ph.SR].
 - [18] A. Bauswein, N. Stergioulas, and H. T. Janka, Revealing the high-density equation of state through binary neutron star mergers, *Phys. Rev. D* **90**, 023002 (2014), arXiv:1403.5301 [astro-ph.SR].
 - [19] A. Bauswein, S. Blacker, G. Lioutas, T. Soutanis, V. Vijayan, and N. Stergioulas, Systematics of prompt black-

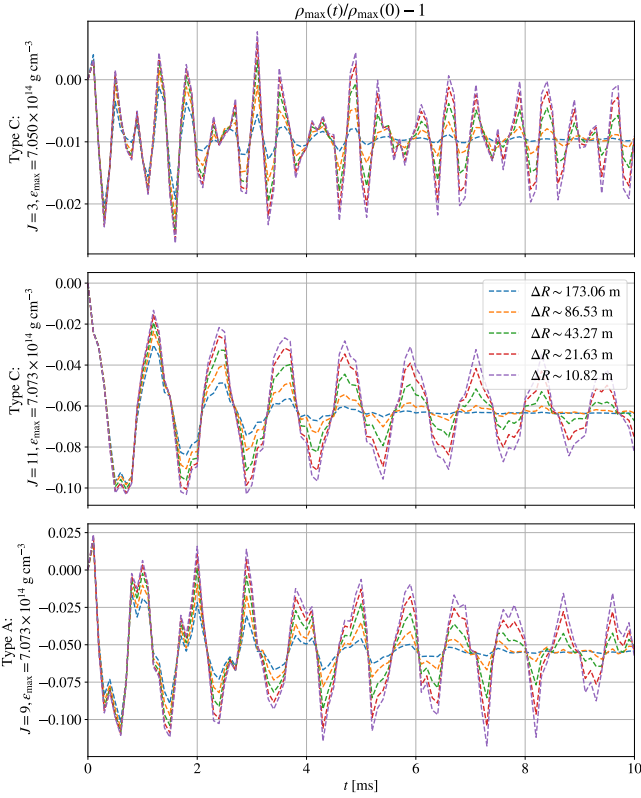


FIG. 8. The relative variation of the maximum rest mass density ρ_{\max} with different resolution in different models. *Upper panel*: Quasi-toroidal (type C) model with $J = 3$ $\epsilon_{\max} = 7.050 \times 10^{14} \text{ g} \cdot \text{cm}^{-3}$. *Middle panel*: Quasi-toroidal (type C) model with $J = 11$ $\epsilon_{\max} = 7.073 \times 10^{14} \text{ g} \cdot \text{cm}^{-3}$. *Lower panel*: Quasi-spherical (type A) model with $J = 9$ $\epsilon_{\max} = 7.073 \times 10^{14} \text{ g} \cdot \text{cm}^{-3}$. Initial in-going velocity perturbation is introduced in these simulations. As shown in the plot, the oscillation amplitudes are mostly the same at the very beginning, and gradually decrease as time goes on. At low resolution, the simulations are very diffusive, which relax the oscillation sooner.

hole formation in neutron star mergers, *Phys. Rev. D* **103**, 123004 (2021), arXiv:2010.04461 [astro-ph.HE].

[20] G. Lioutas, A. Bauswein, T. Soutanis, R. Pakmor, V. Springel, and F. K. Röpke, General relativistic moving-mesh hydrodynamic simulations with AREPO and applications to neutron star mergers, *MNRAS* **528**, 1906 (2024), arXiv:2208.04267 [astro-ph.HE].

[21] H. Dimmelmeier, J. A. Font, and E. Müller, Relativistic simulations of rotational core collapse II. Collapse dynamics and gravitational radiation, *Astron. Astrophys.* **393**, 523 (2002), arXiv:astro-ph/0204289 [astro-ph].

[22] M. Saijo, The Collapse of Differentially Rotating Supermassive Stars: Conformally Flat Simulations, *Astrophys. J.* **615**, 866 (2004), astro-ph/0407621.

[23] B. Müller, The dynamics of neutrino-driven supernova explosions after shock revival in 2D and 3D, *Mon. Not. Roy. Astron. Soc.* **453**, 287 (2015), arXiv:1506.05139 [astro-ph.SR].

[24] H. Dimmelmeier, N. Stergioulas, and J. A. Font, Non-linear axisymmetric pulsations of rotating relativistic

stars in the conformal flatness approximation, *Mon. Not. Roy. Astron. Soc.* **368**, 1609 (2006), arXiv:astro-ph/0511394 [astro-ph].

[25] Bucciantini, N. and Del Zanna, L., General relativistic magnetohydrodynamics in axisymmetric dynamical spacetimes: the x-echo code, *A&A* **528**, A101 (2011).

[26] H. H.-Y. Ng, P. C.-K. Cheong, L.-M. Lin, and T. G. F. Li, Gravitational-wave Asteroseismology with f-modes from Neutron Star Binaries at the Merger Phase, *ApJ* **915**, 108 (2021), arXiv:2012.08263 [astro-ph.HE].

[27] M. Y. Leung, A. K. L. Yip, P. C.-K. Cheong, and T. G. F. Li, Oscillations of highly magnetized non-rotating neutron stars, *Communications Physics* **5**, 334 (2022), arXiv:2303.05684 [astro-ph.HE].

[28] A. K. L. Yip, P. Chi-Kit Cheong, and T. G. F. Li, General-relativistic simulations of the formation of a magnetized hybrid star, arXiv e-prints, arXiv:2303.16820 (2023), arXiv:2303.16820 [astro-ph.HE].

[29] A. K. L. Yip, P. Chi-Kit Cheong, and T. G. F. Li, Universal relations for fundamental modes of rotating neutron stars with differential rotations, arXiv e-prints, arXiv:2401.13993 (2024), arXiv:2401.13993 [astro-ph.HE].

[30] N. Bucciantini and L. Del Zanna, General relativistic magnetohydrodynamics in axisymmetric dynamical spacetimes: the X-ECHO code, *A&A* **528**, A101 (2011), arXiv:1010.3532 [astro-ph.IM].

[31] A. G. Pili, N. Bucciantini, and L. Del Zanna, Axisymmetric equilibrium models for magnetized neutron stars in General Relativity under the Conformally Flat Condition, *MNRAS* **439**, 3541 (2014), arXiv:1401.4308 [astro-ph.HE].

[32] A. G. Pili, N. Bucciantini, and L. Del Zanna, General relativistic neutron stars with twisted magnetosphere, *MNRAS* **447**, 2821 (2015), arXiv:1412.4036 [astro-ph.HE].

[33] A. G. Pili, N. Bucciantini, and L. Del Zanna, General relativistic models for rotating magnetized neutron stars in conformally flat space-time, *MNRAS* **470**, 2469 (2017), arXiv:1705.03795 [astro-ph.HE].

[34] J. Soldateschi, N. Bucciantini, and L. Del Zanna, Axisymmetric equilibrium models for magnetised neutron stars in scalar-tensor theories, *A&A* **640**, A44 (2020), arXiv:2005.12758 [astro-ph.HE].

[35] S. Fujibayashi, Y. Sekiguchi, K. Kiuchi, and M. Shibata, Properties of Neutrino-driven Ejecta from the Remnant of a Binary Neutron Star Merger: Pure Radiation Hydrodynamics Case, *ApJ* **846**, 114 (2017), arXiv:1703.10191 [astro-ph.HE].

[36] H. Ho-Yin Ng, J.-L. Jiang, C. Musolino, C. Ecker, S. D. Tootle, and L. Rezzolla, A hybrid approach to long-term binary neutron-star simulations, arXiv e-prints, arXiv:2312.11358 (2023), arXiv:2312.11358 [gr-qc].

[37] P. C.-K. Cheong, L.-M. Lin, and T. G. F. Li, Gmunu: toward multigrid based Einstein field equations solver for general-relativistic hydrodynamics simulations, *Classical and Quantum Gravity* **37**, 145015 (2020), arXiv:2001.05723 [gr-qc].

[38] P. C.-K. Cheong, A. T.-L. Lam, H. H.-Y. Ng, and T. G. F. Li, Gmunu: paralleled, grid-adaptive, general-relativistic magnetohydrodynamics in curvilinear geometries in dynamical space-times, *MNRAS* **508**, 2279 (2021), arXiv:2012.07322 [astro-ph.IM].

[39] A. Garat and R. H. Price, Nonexistence of conformally flat slices of the Kerr spacetime, *Phys. Rev. D* **61**, 124011

- (2000), arXiv:gr-qc/0002013 [gr-qc].
- [40] J. A. Kroon, Nonexistence of Conformally Flat Slices in Kerr and Other Stationary Spacetimes, *Phys. Rev. Lett.* **92**, 041101 (2004), arXiv:gr-qc/0310048 [gr-qc].
- [41] G. B. Cook, S. L. Shapiro, and S. A. Teukolsky, Testing a simplified version of Einstein's equations for numerical relativity, *Phys. Rev. D* **53**, 5533 (1996), arXiv:gr-qc/9512009 [gr-qc].
- [42] P. Iosif and N. Stergioulas, On the accuracy of the IWM-CFC approximation in differentially rotating relativistic stars, *General Relativity and Gravitation* **46**, 1800 (2014), arXiv:1406.7375 [gr-qc].
- [43] P. Iosif and N. Stergioulas, Equilibrium sequences of differentially rotating stars with post-merger-like rotational profiles, *MNRAS* **503**, 850 (2021), arXiv:2011.10612 [gr-qc].
- [44] P. Iosif and N. Stergioulas, Models of binary neutron star remnants with tabulated equations of state, *MNRAS* **510**, 2948 (2022), arXiv:2104.13672 [astro-ph.HE].
- [45] J. L. Friedman, J. R. Ipser, and R. D. Sorkin, Turning Point Method for Axisymmetric Stability of Rotating Relativistic Stars, *ApJ* **325**, 722 (1988).
- [46] P. Szweczyk, D. Gondek-Rosińska, and P. Cerdá-Durán, Maximum mass and stability of differentially rotating neutrons stars, arXiv e-prints, arXiv:2302.06007 (2023), arXiv:2302.06007 [astro-ph.HE].
- [47] G. B. Cook, S. L. Shapiro, and S. A. Teukolsky, Rapidly Rotating Polytropes in General Relativity, *ApJ* **422**, 227 (1994).
- [48] K. Uryū, S. Yoshida, E. Gourgoulhon, C. Markakis, K. Fujisawa, A. Tsokaros, K. Taniguchi, and Y. Eriguchi, New code for equilibriums and quasiequilibrium initial data of compact objects. IV. Rotating relativistic stars with mixed poloidal and toroidal magnetic fields, *Phys. Rev. D* **100**, 123019 (2019), arXiv:1906.10393 [gr-qc].
- [49] N. Muhammed, M. D. Duez, P. Chawhan, N. Ghadiri, L. T. Buchman, F. Foucart, P. Chi-Kit Cheong, L. E. Kidder, H. P. Pfeiffer, and M. A. Scheel, Stability of hypermassive neutron stars with realistic rotation and entropy profiles, arXiv e-prints, arXiv:2403.05642 (2024), arXiv:2403.05642 [gr-qc].
- [50] M. Ansorg, D. Gondek-Rosińska, and L. Villain, On the solution space of differentially rotating neutron stars in general relativity, *MNRAS* **396**, 2359 (2009), arXiv:0812.3347 [gr-qc].
- [51] M. Hanauske, K. Takami, L. Bovard, L. Rezzolla, J. A. Font, F. Galeazzi, and H. Stöcker, Rotational properties of hypermassive neutron stars from binary mergers, *Phys. Rev. D* **96**, 043004 (2017), arXiv:1611.07152 [gr-qc].
- [52] R. De Pietri, A. Feo, J. A. Font, F. Löffler, M. Pasquali, and N. Stergioulas, Numerical-relativity simulations of long-lived remnants of binary neutron star mergers, *Phys. Rev. D* **101**, 064052 (2020), arXiv:1910.04036 [gr-qc].
- [53] M. Hempel and J. Schaffner-Bielich, A statistical model for a complete supernova equation of state, *Nucl. Phys. A* **837**, 210 (2010), arXiv:0911.4073 [nucl-th].
- [54] P. C.-K. Cheong, D. Y. T. Pong, A. K. L. Yip, and T. G. F. Li, An Extension of Gmumu: General-relativistic Resistive Magnetohydrodynamics Based on Staggered-meshed Constrained Transport with Elliptic Cleaning, *ApJS* **261**, 22 (2022), arXiv:2110.03732 [astro-ph.IM].
- [55] P. C.-K. Cheong, H. H.-Y. Ng, A. T.-L. Lam, and T. G. F. Li, General-relativistic Radiation Transport Scheme in Gmumu. I. Implementation of Two-moment-based Multi-frequency Radiative Transfer and Code Tests, *ApJS* **267**, 38 (2023), arXiv:2303.03261 [astro-ph.IM].
- [56] H. Ho-Yin Ng, P. C.-K. Cheong, A. Tsz-Lok Lam, and T. G. F. Li, General-relativistic radiation transport scheme in Gmumu II: Implementation of novel micro-physical library for neutrino radiation – Weakhub, arXiv e-prints, arXiv:2309.03526 (2023), arXiv:2309.03526 [astro-ph.HE].
- [57] A. Harten, P. Lax, and B. Leer, On upstream differencing and godunov-type schemes for hyperbolic conservation laws, *SIAM Review* **25**, 35 (1983), <https://doi.org/10.1137/1025002>.
- [58] P. Colella and P. R. Woodward, The Piecewise Parabolic Method (PPM) for Gas-Dynamical Simulations, *Journal of Computational Physics* **54**, 174 (1984).
- [59] C.-W. Shu and S. Osher, Efficient Implementation of Essentially Non-oscillatory Shock-Capturing Schemes, *Journal of Computational Physics* **77**, 439 (1988).
- [60] L. R. Weih, E. R. Most, and L. Rezzolla, On the stability and maximum mass of differentially rotating relativistic stars, *MNRAS* **473**, L126 (2018), arXiv:1709.06058 [gr-qc].
- [61] P. L. Espino, V. Paschalidis, T. W. Baumgarte, and S. L. Shapiro, Dynamical stability of quasispherical differentially rotating neutron stars, *Phys. Rev. D* **100**, 043014 (2019), arXiv:1906.08786 [astro-ph.HE].
- [62] SpEC: Spectral einstein code, <https://www.black-holes.org/code/SpEC.html>, [Accessed Feb. 27, 2024].
- [63] J. Jesse, M. D. Duez, F. Foucart, M. Haddadi, A. L. Knight, C. L. Cadenhead, F. Hébert, L. E. Kidder, H. P. Pfeiffer, and M. A. Scheel, Axisymmetric hydrodynamics in numerical relativity using a multipatch method, *Classical and Quantum Gravity* **37**, 235010 (2020), arXiv:2005.01848 [gr-qc].
- [64] K. N. Gourgouliatos and S. S. Komissarov, Relativistic centrifugal instability, *MNRAS* **475**, L125 (2018), arXiv:1710.01345 [astro-ph.HE].
- [65] M. J. Turk, B. D. Smith, J. S. Oishi, S. Skory, S. W. Skillman, T. Abel, and M. L. Norman, yt: A Multi-code Analysis Toolkit for Astrophysical Simulation Data, *The Astrophysical Journal Supplement Series* **192**, 9 (2011), arXiv:1011.3514 [astro-ph.IM].
- [66] C. R. Harris, K. J. Millman, S. J. van der Walt, R. Gommers, P. Virtanen, D. Cournapeau, E. Wieser, J. Taylor, S. Berg, N. J. Smith, R. Kern, M. Picus, S. Hoyer, M. H. van Kerkwijk, M. Brett, A. Haldane, J. F. del Río, M. Wiebe, P. Peterson, P. Gérard-Marchant, K. Sheppard, T. Reddy, W. Weckesser, H. Abbasi, C. Gohlke, and T. E. Oliphant, Array programming with NumPy, *Nature* **585**, 357 (2020).
- [67] T. pandas development team, pandas-dev/pandas: Pandas (2020).
- [68] Wes McKinney, Data Structures for Statistical Computing in Python, in *Proceedings of the 9th Python in Science Conference*, edited by Stéfan van der Walt and Jarrod Millman (2010) pp. 56 – 61.
- [69] P. Virtanen, R. Gommers, T. E. Oliphant, M. Haberland, T. Reddy, D. Cournapeau, E. Burovski, P. Peterson, W. Weckesser, J. Bright, S. J. van der Walt, M. Brett, J. Wilson, K. J. Millman, N. Mayorov, A. R. J.

- Nelson, E. Jones, R. Kern, E. Larson, C. J. Carey, Í. Polat, Y. Feng, E. W. Moore, J. VanderPlas, D. Laxalde, J. Perktold, R. Cimrman, I. Henriksen, E. A. Quintero, C. R. Harris, A. M. Archibald, A. H. Ribeiro, F. Pedregosa, P. van Mulbregt, and SciPy 1.0 Contributors, SciPy 1.0: Fundamental Algorithms for Scientific Computing in Python, *Nature Methods* **17**, 261 (2020).
- [70] J. D. Hunter, Matplotlib: A 2D Graphics Environment, *Computing in Science and Engineering* **9**, 90 (2007).
- [71] T. A. Caswell, A. Lee, E. S. de Andrade, M. Droettboom, T. Hoffmann, J. Klymak, J. Hunter, E. Firing, D. Stansby, N. Varoquaux, J. H. Nielsen, B. Root, R. May, O. Gustafsson, P. Elson, J. K. Seppänen, J.-J. Lee, D. Dale, hannah, D. McDougall, A. Straw, P. Hobson, K. Sunden, G. Lucas, C. Gohlke, A. F. Vincent, T. S. Yu, E. Ma, S. Silvester, and C. Moad, matplotlib/matplotlib: Rel: v3.7.1 (2023).